ADVANCED FUNCTIONAL MATERIALS
www.afm-journal.de

Overcoming the Trade-off Between Efficient Electrochemical Doping and High State Retention in Electrolyte-Gated Organic Synaptic Transistors

*Min-Jun Sung, Dae-Gyo Seo, Jingwan Kim, Ho Eon Baek, Gyeong-Tak Go, Seung-Je Woo, Kwan-Nyeong Kim, Hoichang Yang, Yun-Hi Kim, and Tae-Woo Lee**

To achieve superior device performance such as low threshold voltage V_{th}, high maximum on-current $I_{on,max}$, and long retention time in electrolyte-gated organic synaptic transistors, efficient electrochemical doping and high state retention are essential. However, these characteristics generally show a trade-off relationship. This work introduces an effective strategy to increase retention time while promoting efficient electrochemical doping. The approach involves blending two polymer semiconductors (PSCs) that have the same backbone but different types of side chains. Polymer synaptic transistors (PSTs) with the blend film showed the lowest V_{th}, highest $I_{on,max}$, longest retention time, and superior cyclic stability compared to PSTs that used films containing only one of the PSCs. The improvement in electrical and synaptic properties achieved through the blend strategy is consistently reproducible and comprehensive. It is attributed this improvement to the increased redox activity and constrained morphological changes observed in the blended PSCs during electrochemical doping, as confirmed by several electrochemical characterizations. This work is the first to increase retention time in PSTs without increasing the crystallinity of polymer film or sacrificing the electrochemical doping efficiency, which has been regarded as an unavoidable compromise in this field. This method provides an effective way to tune synaptic properties for various neuromorphic applications.

1. Introduction

Organic neuromorphic devices (ONDs) have been suggested as an alternative to conventional inorganic neuromorphic devices due to the inherent properties of organic semiconductors (OSCs) including organic small molecules and polymers.[1–3] OSCs have mechanical and electrical properties that can be easily tuned over a wide range by tailoring their molecular structure, thus enabling ONDs to exhibit controllable synaptic plasticity.[4,5] Among various ONDs, electrolyte-gated organic synaptic transistors (EGOSTs) have useful features such as less-stochastic switching compared to conventional inorganic memristors, a large ratio of "on" current I_{on} to "off" current I_{off} (I_{on}/I_{off}), and low operating voltage due to the electrochemical doping mechanism.[6–9] Specifically, ion-gel dielectric, which can be prepared from mixtures of an ionic liquid and a polyelectrolyte is promising because it can endow synaptic transistors with long-term stability, large electrochemical window, high capacitance, and compatibility with lithography procedure.[10–12] The devices can emulate the transmission of action potentials, which occurs by the release and uptake of neurotransmitters in biological synapses.[13] This emulation occurs as a change in the channel conductance by inserting ions into the OSC channel and extracting ions from it. In ion-permeable p-type OSCs, anions can be doped into the channel by a negative bias applied to the top of the electrolyte (**Figure 1a**). This electrochemical doping induces

M.-J. Sung, D.-G. Seo, G.-T. Go, S.-J. Woo, K.-N. Kim, T.-W. Lee
Department of Materials Science and Engineering
Seoul National University
1 Gwanak-ro, Gwanak-gu, Seoul 08826, Republic of Korea
E-mail: twlees@snu.ac.kr

J. Kim, H. E. Baek, Y.-H. Kim
Department of Chemistry and Research Institute of Green Energy Convergence Technology (RIGET)
Gyeongsang National University
501 Jinju-daero, Jinju, Gyeongnam 52828, Republic of Korea

H. Yang
Department of Chemical Engineering
Inha University
100 Inha-ro, Michuhol-gu, Incheon 22212, Republic of Korea

T.-W. Lee
School of Chemical and Biological Engineering
Institute of Engineering Research
Research Institute of Advanced Materials
Nano Systems Institute (NSI)
Seoul National University
1 Gwanak-ro, Gwanak-gu, Seoul 08826, Republic of Korea

The ORCID identification number(s) for the author(s) of this article can be found under https://doi.org/10.1002/adfm.202312546

DOI: 10.1002/adfm.202312546

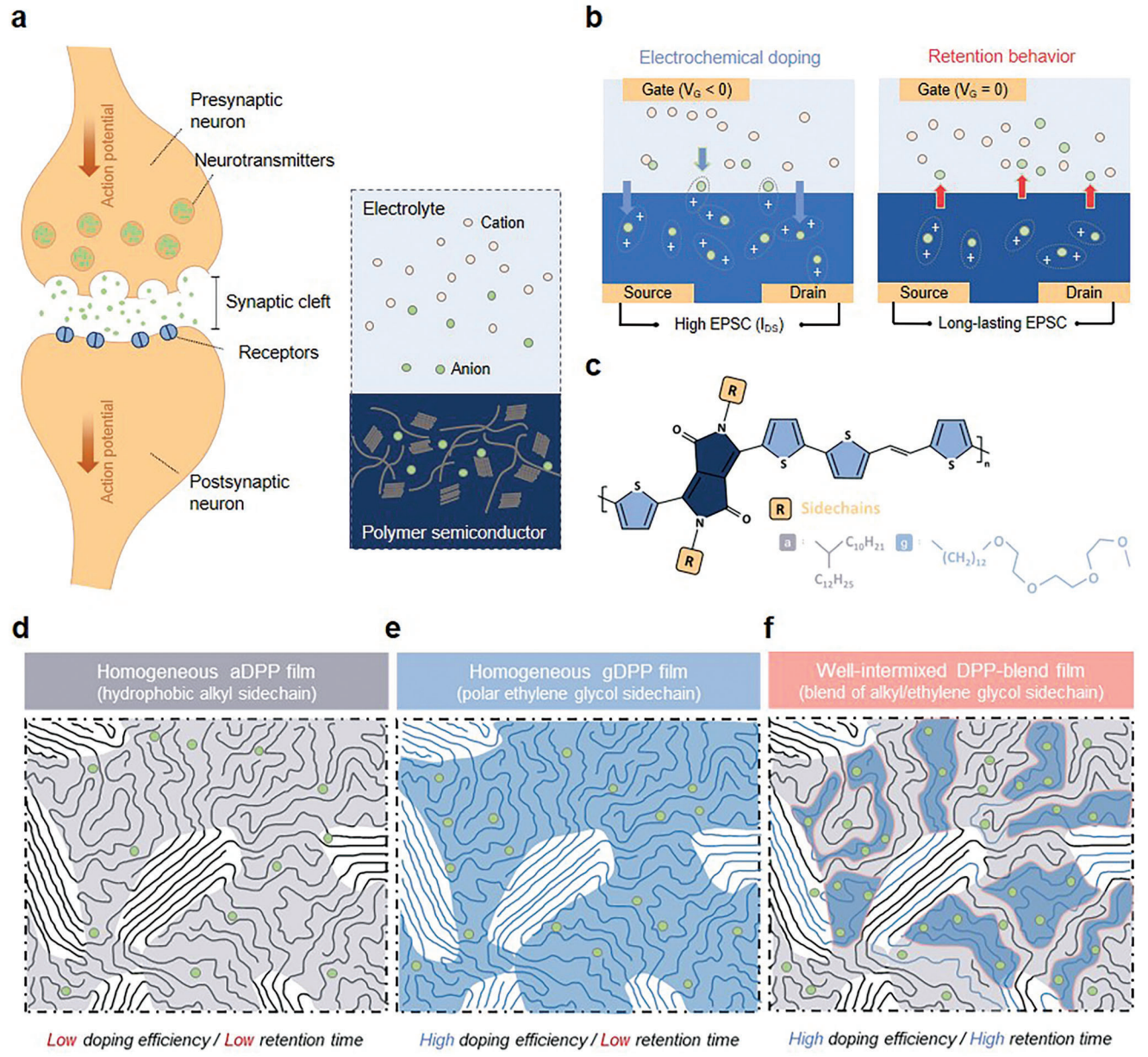

Figure 1. a) Schematics of a biological synapse and electrolyte-gating mechanism that mimics a biological synapse. b) Device structure of ion-gel gated polymer synaptic transistors (IGPSTs); electrochemical doping occurred with negative gate voltage V_G, and retention behavior occurred at $V_G = 0$. c) Chemical structures of donor-acceptor backbone and side chains of synthesized DPP copolymers. Branched alkyl side chains [a] are attached to aDPP copolymers, whereas triethylene glycol side chains with alkyl spacer [g] are attached to gDPP copolymers. d–f) Schematics of electrochemical doping efficiency and retention time in different ion-conducting environments. Both electrochemical doping efficiency and retention time are relatively poor due to the hydrophobic environment of alkyl side chains (left image). Polar ethylene glycol side chains enable gDPP film to have high electrochemical doping efficiency, but gDPP film still shows low redox activity (middle image). In the blend system, efficient electrochemical doping and high state retention is achieved simultaneously (right image). White areas: ordered regions of PSCs. colored areas: disordered regions of PSCs.

hole compensation through the channel and thereby increases the channel conductance, so drain current I_{DS} increases. I_{DS} is also referred to as excitatory post-synaptic current (EPSC) in the field of neuromorphic electronics. However, the devices usually suffer from limited retention of EPSC because doped ions spontaneously diffuse back from the channel layer to the initial distribution in the electrolyte. This phenomenon limits the emulation of brain-like functionalities required in neuromorphic electronics, especially in terms of long-term potentiation (LTP). Thus, demonstrating both efficient electrochemical doping and high state retention is a crucial requirement in EGOSTs (Figure 1b).

Several methods have been used to modulate the synaptic properties by controlling the crystallinity of polymer semiconductors (PSCs) in EGOSTs. For instance, self-assembly monolayer treatment, high annealing temperature, and solvent engineering increase crystallinity and can increase the retention time T_{rtn} of

LTP.[5,14,15] The crystalline region has been considered as a barrier to the spontaneous de-doping of ions trapped in the PSC channel. The introduction of ion-blocking polymer or ion-conducting polyelectrolyte into PSCs has been also evaluated to modulate synaptic properties.[16,17] However, these approaches can sacrifice either electrochemical doping efficiency η_{echem} or T_{rtn} of LTP because there is a trade-off between the two characteristics; easier electrochemical doping can lead to faster de-doping of ions, on the other hand, retarding de-doping of ions can limit η_{echem}.

In this work, we designed a well-intermixed polymer blend of two PSCs with different side chains to achieve long-term synaptic plasticity with no sacrifice in η_{echem}. Synaptic properties were evaluated in solidified ion-gel-gated polymer synaptic transistors (IGPSTs) that used films fabricated using each PSC component or blended PSC. We synthesized two copolymers derived from diketopyrrolopyrrole (DPP) with the same procedures;[18,19] they contained vinylene with thiophene as a donor unit (TTVTT) plus either a branched alkyl side chain (aDPP) or a triethylene glycol end-group with alkyl spacer (gDPP) (Figure 1c). In the electrochemical operation of IGPSTs, hydrophobic alkyl side chains create a poor ion-conducting environment, so aDPP film has low η_{echem} (Figure 1d). On the other hand, ions can be easily doped in gDPP film because polar ethylene glycol groups facilitate easy access of ions to the doping sites by providing an ion hopping mechanism (Figure 1e). In both IGPSTs that use each PSC film, weak redox reactions and corresponding short T_{rtn} were observed. However, we found that both efficient electrochemical doping and high state retention were simultaneously achieved in the blend film (Figure 1f). IGPSTs that used the blend film had lower V_{th}, higher $I_{on,max}$, higher transconductance g_m, and higher operational stability than IGPSTs that used films composed of only one of the polymers. Furthermore, in the synaptic properties, IGPSTs that used the blend film exhibited stronger potentiation under weaker presynaptic spikes and retained EPSC longer than the other IGPSTs. With in situ UV-vis spectroscopy and cyclic voltammetry, we identified that stronger redox reactions occurred in the blend film than in each single-polymer film. This phenomenon might be attributed to the improved physical interaction between polymer chains and ions caused by limited morphological change upon electrochemical doping, which was observed ex-situ electrochemical atomic force microscopy (EC-AFM). Additionally, the aDPP and gDPP copolymers were well intermixed in the blend film, with backbone stacking and electronic charge transport being maintained. The blend film had the lowest crystallinity while it shows the longest T_{rtn} of LTP; this result implies that the extended T_{rtn} of LTP did not originate from the change of crystallinity in this study, which has been previously suggested as a method to modulate synaptic plasticity. In recognition simulations of MNIST handwritten digits, the IGPST with the blend film achieved a high training accuracy of 96.8%, which nearly approaches the ideal numerical value of 98.2%.

2. Results

IGPSTs were fabricated using aDPP film alone ($IGPST_A$), gDPP film alone ($IGPST_G$), or with DPP-blend film ($IGPST_{A+G}$) to investigate the change in synaptic properties depending on the distribution of side chains. DPP-blend thin film was spin-coated from a solution composed of aDPP and gDPP copolymers (5:5, w:w) in chloroform (5 mg mL^{-1}), using the same deposition parameters as those used for aDPP and gDPP thin films.

First, transfer curves were measured starting from gate voltage $V_G = 3.5$ V (de-potentiation) to $V_G = -3.5$ V (potentiation) in the IGPSTs (**Figure 2a**). To ensure statistical validity, five distinct devices on each DPP polymer film were utilized for the measurement (Figure S2, Supporting Information). Crucial quantitative index such as the threshold voltage V_{th}, maximum on-current $I_{on,max}$, hysteresis window ΔV_{hys}, and normalized transconductance $g_m(NR)$ are evaluated to compare the electrical characteristics of the IGPSTs (Figure 2b and Table S1, Supporting Information). ΔV_{hys} was determined by measuring the voltage difference at which the drain current reaches half of $I_{on,max}$ during forward and backward sweeps. $IGPST_G$ showed less-negative V_{th} and increased $I_{on,max}$ compared to $IGPST_A$. The differences are attributed to the easier electrochemical doping in the glycolated side chains of gDPP than in the alkyl side chains of aDPP.[19,20] Notably, $IGPST_{A+G}$ showed the least-negative $V_{th} = -2.8$ V and highest $|I_{on,max}| > 600$ μA, which is a 230% increase compared to $IGPST_A$ and a 50% increase compared to $IGPST_G$. This result indicates that electrochemical doping and charge injection became easy in the blend film.[21] Furthermore, the widest ΔV_{hys} was observed in the transfer curve of $IGPST_{A+G}$, indicating that back-diffusion of anions doped in the channel was decelerated in the blend film. The widened hysteresis suggests that the blending method may increase the retention time T_{rtn} of LTP.

The transconductance g_m and its normalized value to the channel dimension $g_m(NR)$ are calculated as

$$g_m = \frac{\partial I_D}{\partial V_G}, \quad g_m(NR) = g_m \div \frac{Wd}{L} \tag{1}$$

where $W = 1.5$ mm is channel width, d is channel thickness, and $L = 50$ μm is channel length.[22] d was 40 nm for aDPP film, 35 nm for gDPP film, and 45 nm for DPP-blend film. $IGPST_{A+G}$ had a higher average $g_m(NR) = 8.7$ S cm^{-1} than $IGPST_A$ and $IGPST_G$. This result indicates that blending two PSCs that have the same backbone but different side chains can increase the electrochemical doping efficiency η_{echem}.

Cyclic transfer curves with 100 consecutive cycles were measured to confirm the cyclic stability of the IGPSTs. $I_{on,max}$ and ΔV_{hys} were well maintained across all three IGPSTs over the total cyclic operation (Figure S3a, Supporting Information). The gradual decrease of $I_{on,max}$ in the cycling test is attributed to irreversible changes in the polymeric microstructures, or the presence of irreversible reactions, or both.[23] Moreover, the residual solvent, in this case acetone, can persist in the ion gel, then infiltrate the polymer films during the doping of ionic species while the device operates, and thereby lead to irreversible swelling, which is particularly prominent in the gDPP films because they contain polar ethylene glycol groups. However, despite the evident change in $I_{on,max}$ in the IGPSTs, the drop-off was comparatively slow in $IGPST_{A+G}$, and it maintained stable transfer curves (Figure S3b, Supporting Information). These data suggest that the blend approach enhances both η_{echem} and T_{rtn}, while also contributing to improved cyclic stability.

Short-term potentiation (STP) of the IGPSTs was evaluated by measuring paired pulse facilitation (PPF) with different time intervals Δt between two consecutive presynaptic spikes

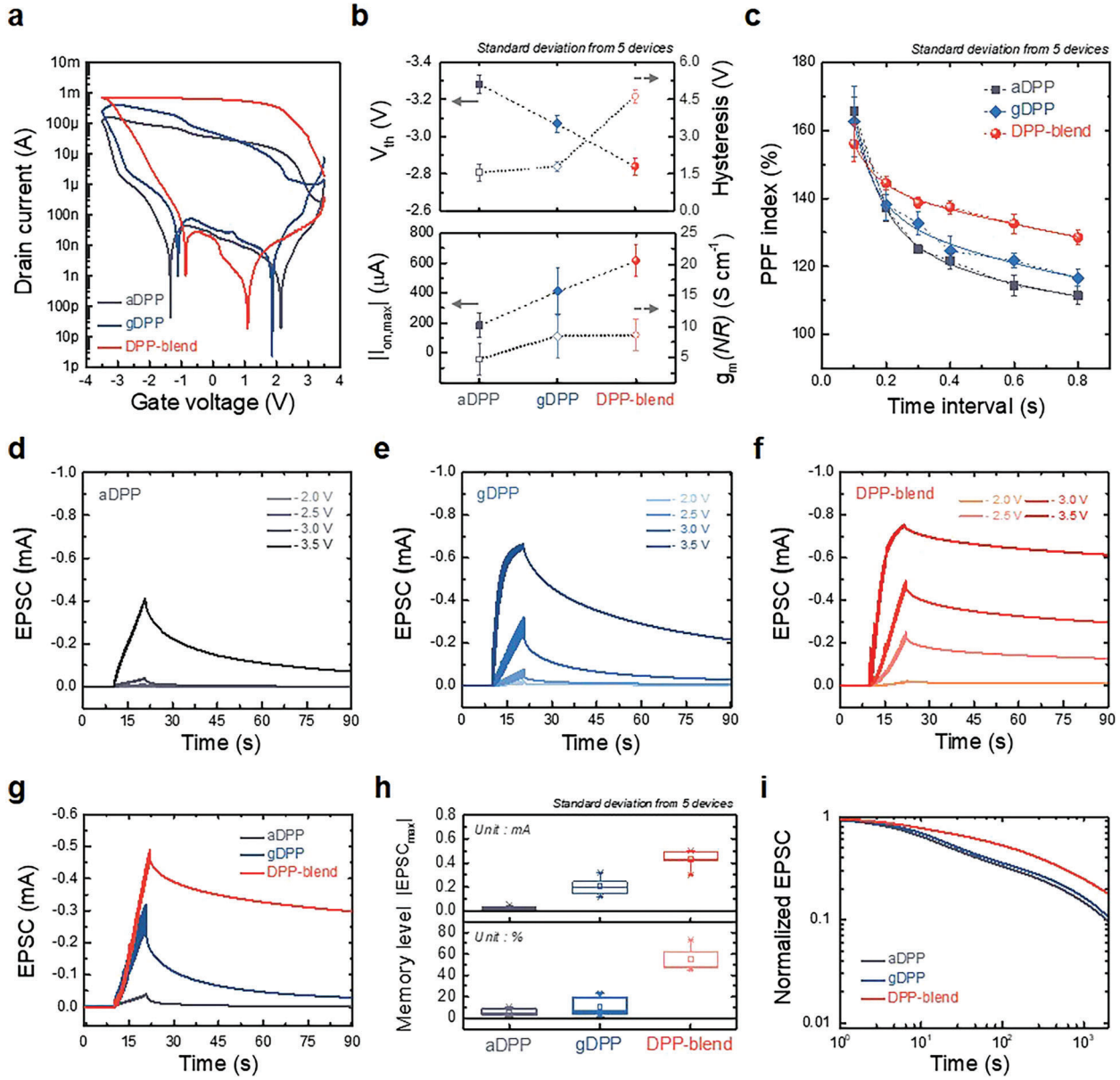

Figure 2. Transfer curves and various synaptic properties of $IGPST_A$ (grey), $IGPST_G$ (blue), and $IGPST_{A+G}$ (red). a) Transfer curves of the IGPSTs. b) Threshold voltage V_{th}, hysteresis window ΔV_{hys}, maximum on-current $I_{on,max}$, and normalized transconductance $g_m(NR)$, which are calculated from the transfer curves. c) Paired pulse facilitation (PPF) index at various time intervals (100, 200, 300, 400, 600, and 800 ms) between two presynaptic spikes. d–f) Spike-amplitude dependent plasticity (SADP) measured with different amplitude (−2.0, −2.5, −3.0, −3.5 V) of presynaptic spikes; 50 spikes were applied, each had duration of 100 ms. Time interval: 100 ms. g) Comparison of synaptic behavior, h) maximum EPSC $EPSC_{max}$, and memory level R_{60} with 50 presynaptic spikes of −3.0 V within IGPSTs. i) Long-term potentiation (LTP) characteristic of the IGPSTs evaluated by observing the decay of EPSC with respect to time after applying 100 presynaptic spikes of −3.5 V and 100 ms. All synaptic properties were characterized using $V_D = -100$ mV. Grey square: $IGPST_A$, blue rhombus: $IGPST_G$, red circle: $IGPST_{A+G}$.

(Figure 2c). PPF represents an increase in the amplitude A_2 of the excitatory post-synaptic current (EPSC) after the second stimulus, compared to the amplitude A_1 of the EPSC after the first stimulus; the change is quantified as a percentage by using the PPF index $I_{PPF} = 100 \times A_2/A_1$ (%). If a single stimulus is applied, ions that are driven into the PSC film rapidly diffuse back to their original distribution in the ion gel. PPF occurs when a second stimulus arrives before this back-diffusion process finishes and is strongest at small Δt because it is associated with residual anions in the PSC channel. As Δt increases, I_{PPF} decays can be expressed using a double exponential function:

$$I_{\mathrm{PPF}} = 100 + C_1 exp\left(-\Delta t/\tau_1\right) + C_2 exp\left(-\Delta t/\tau_2\right) \quad (\tau_1 < \tau_2) \quad (2)$$

where C_i are proportional contributions and τ_i represent relaxation times (i = 1 for rapid and 2 for slow relaxation).[24] τ_1 was

80 ms for $IGPST_A$, 70 ms for $IGPST_G$, 70 ms for $IGPST_{A+G}$. τ_2 was 710 ms for $IGPST_A$, 870 ms for $IGPST_G$, and 1,600 ms for $IGPST_{A+G}$. The timescales of the PPF decay of the IGPSTs are similar to those of biological synapses and therefore indicate that STP characteristic of the IGPSTs was well established.[24] Moreover, the slowest decay of PPF index in $IGPST_{A+G}$ is indicative of the strengthened synaptic plasticity.

Other synaptic properties including spike-number-dependent plasticity (SNDP) (Figure S4, Supporting Information) and spike-amplitude-dependent plasticity (SADP) (Figure 2d–f and Figure S5a, Supporting Information) were also successfully emulated. Increasing the number or amplitude of presynaptic spikes results in an increase in EPSC (potentiation) and a transition from STP to LTP of IGPSTs; this change emulates a behavior of biological synapses.[25] Moreover, in the SADP characteristic, $IGPST_{A+G}$ showed strong potentiation even under relatively weak potentiation spikes of −2.0 V and −2.5 V, whereas $IGPST_A$ and $IGPST_G$ were barely potentiated. This result originated from the facile electrochemical doping of the blend film, which was confirmed by the trend of V_{th}. Under the same presynaptic spike condition, which is 50 presynaptic spikes with an amplitude of −3.0 V, $IGPST_{A+G}$ showed both the highest maximum EPSC $EPSC_{max}$ and longest retention behavior compared to the other IGPSTs (Figure 2g). For quantitative comparison of SADP characteristics in the IGPSTs, we used $EPSC_{max}$ and memory level, which was defined as $R_{60} = 100 \times EPSC_{60}/EPSC_{max}$ (%) where $EPSC_{60}$ is EPSC after read of 60 s (Figure S5b,c). Furthermore, all measurements for synaptic characteristics were conducted on five devices for each IGPST to account for the device-to-device variation of IGPSTs (Figure S6 and S7, Supporting Information).

At $V_G = -3.0$ V, the $EPSC_{max}$ of $IGPST_{A+G}$ increased by 1400% compared to $IGPST_A$, and by 100% compared to $IGPST_G$; concurrently, R_{60} in $IGPST_{A+G}$ increased by 900% compared to $IGPST_A$ and by 410% compared to $IGPST_G$ (Figure 2h and Table S2, Supporting Information). At $V_G = -3.5$ V, the average $EPSC_{max}$ of $IGPST_{A+G}$ increased by 140% compared to $IGPST_A$, and by 20% compared to $IGPST_G$, although a few $IGPST_G$ devices had $EPSC_{max}$ comparable to those of $IGPST_{A+G}$. Notably, R_{60} was highest in $IGPST_{A+G}$, with an increase of 200% compared to $IGPST_A$ and 130% compared to $IGPST_G$ (Table S2, Supporting Information). The retention behavior can be also analyzed with fit parameters in tri-exponential decay of EPSC (Equation 3),

$$I_{D,norm} = I_{D,norm}^{base} + B_1\exp(-t/\tau_1) + B_2\exp(-t/\tau_2) + B_3\exp(-t/\tau_3),\ (\tau_1 < \tau_2 < \tau_3) \quad (3)$$

where $I_{D,\,norm}$ is normalized EPSC, $I_{D,norm}^{base}$ is normalized off-current I_{off}, t is time, τ_i are relaxation times (1 = depolarization of electron double layer (EDL), 2 = rapid back-diffusion of doped anions, and 3 = slow back-diffusion of doped anions), and B_i are the relative contributions of each relaxation type.[5,26] The important fit parameter is τ_3, which indicates a relaxation time for the most long-lasting EPSC. At $V_G = -3.0$ V, τ_3 in $IGPST_{A+G}$ was 950% higher than in $IGPST_A$ and 240% higher than in $IGPST_G$. Additionally, at $V_G = -3.5$ V, τ_3 in $IGPST_{A+G}$ was 940% higher than in $IGPST_A$ and 640% higher than in $IGPST_G$ (Figure S5d and Table S3, Supporting Information).

The LTP characteristic of the IGPSTs was further evaluated, and as a result, $IGPST_{A+G}$ showed longer-lasting LTP than $IGPST_A$ and $IGPST_G$ (Figure 2i and Figure S8, Supporting Information). After applying 50 presynaptic spikes of −3.5 V, $IGPST_{A+G}$ maintained > 20% of its initial EPSC, but $IGPST_A$ and $IGPST_G$ decayed to < 10% of their initial EPSCs within the measurement time (2000 s). Consistent with the comparison of fit parameters among the IGPSTs addressed in the SADP characteristic, $IGPST_{A+G}$ showed the highest τ_3 and B_3 (i.e., the number of doped anions that undergo slow back-diffusion was higher in blend film than in films that had only one PSC.

In summary, the statistical and quantitative comparison of electrochemical doping efficiency involved $I_{on,max}$, $g_m(NR)$ from the transfer curve, and $EPSC_{max}$ from synaptic property measurements. All quantities were enhanced in $IGPST_{A+G}$: $I_{on,max}$ by 50 to 230%, $g_m(NR)$ by up to 80%, and $EPSC_{max}$ by 100 to 1400%. To assess retention behavior, we used ΔV_{hys} from the transfer curve, the fit parameters during EPSC decay, and the memory level R_{60}. The blend strategy increased ΔV_{hys} by up to 300%, increased R_{60} by 130 to 900%, and increased τ_3 by 240 to 950% (Figure S9, Supporting Information). To confirm the independence of the blend strategy from the physical properties of synthesized PSCs (i.e., M_n, M_w, and PDI), we synthesized a new batch of gDPP copolymer with higher M_w and PDI than the previous batch of gDPP (Figure S10, Supporting Information). Quantitative comparisons, including $EPSC_{max}$ and R_{60}, supported the enhancement in electrochemical doping efficiency and retention time (Figure S11, Supporting Information). Furthermore, two new PSCs, employing the same side chain engineering strategy with DPP copolymers, were synthesized to validate the generality of the blend strategy. Irrespective of the PSC types, the blend film exhibited more efficient electrochemical doping and higher state retention in the IGPST (Figure S12, Supporting Information). These consistent trends in both doping and de-doping behaviors align with previous results, confirming the generality of the blend strategy in ion-gel-gated synaptic devices.

Optical and electrochemical properties of each DPP copolymer film confirmed the impeded back-diffusion of doped anions in $IGPST_{A+G}$. All DPP copolymer films showed similar absorption spectra with a weak π-π^* transition band around wavelength $400 \le \lambda \le 500$ nm and a strong intramolecular charge-transfer band around $550 \le \lambda \le 1050$ nm (Figure S13, Supporting Information).[19,27] In situ electrochemical UV-vis spectroscopy was conducted to observe the formation and decay of polaronic species during the electrochemical reaction of polymer films (Figure S14, Supporting Information). A continuous bias of −2.5 V was applied to solidified ion gel for 40 s to electrochemically dope anions into polymer films. Therefore, in this doping regime (t < 40 s), the intramolecular charge-transfer band quenched and absorbance above the wavelength of ≈950 nm increased; this change indicates the formation of polaronic species (Figure S15a, Supporting Information). Subsequently, 0 V was applied, to permit decay of polaronic species and recovery of neutral species associated with the spontaneous back-diffusion of doped anions. In this de-doping regime (t > 40 s), the changed absorption spectrum recovered to its original spectrum as the de-doping time increased (Figure S15b, Supporting Information).[28] The in situ electrochemical UV-vis spectra of polymer films showed complementary time trends in

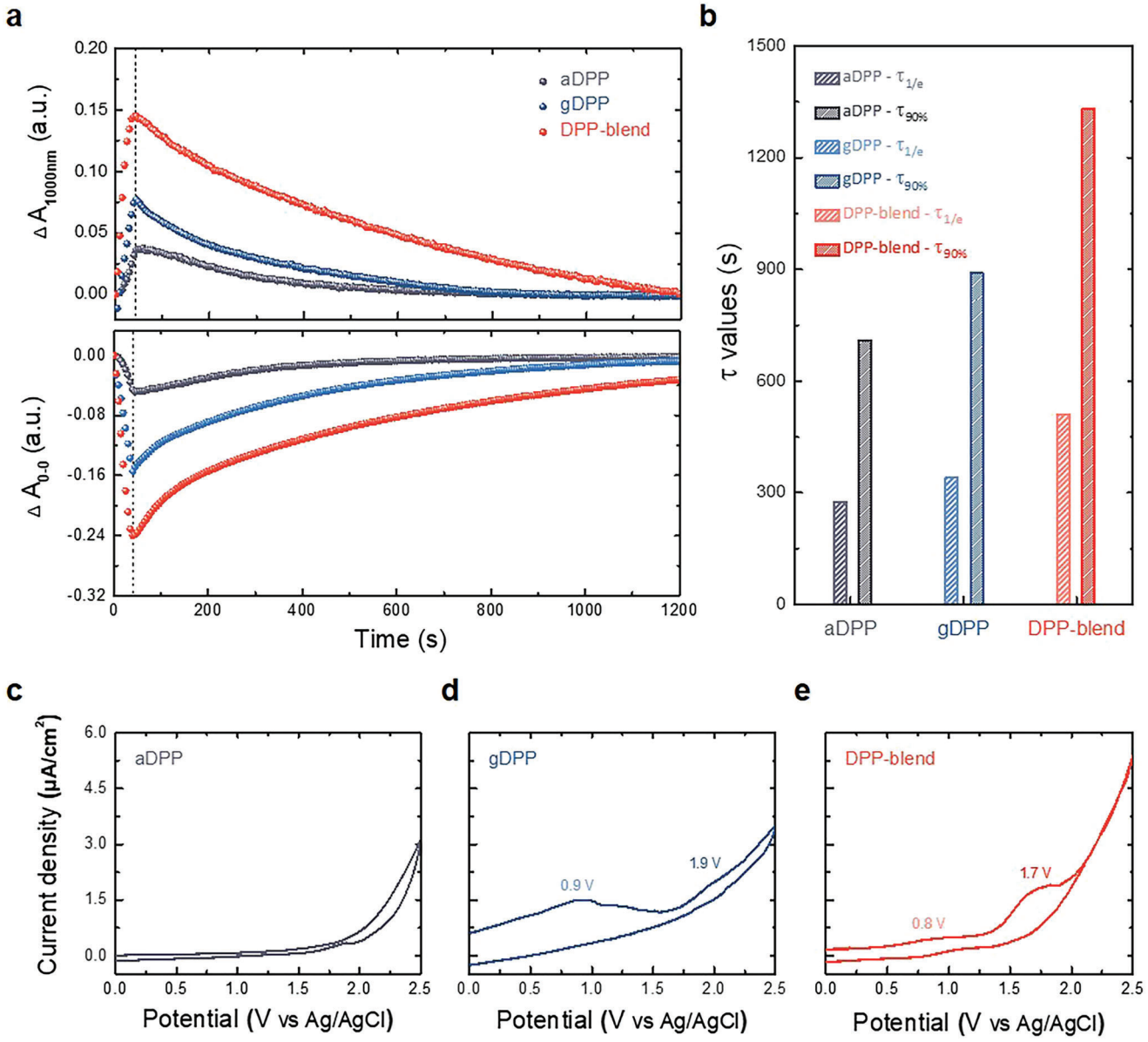

Figure 3. Optical and electrochemical properties of aDPP (grey), gDPP (blue), and DPP-blend (red) films. a) The changes in absorbance at 0-0 transition peak $\Delta A_{0\text{-}0}$ and at wavelength of 1000 nm $\Delta A_{1000\ nm}$ during electrochemical doping ($t < 40$ s) and spontaneous de-doping ($t > 40$ s). b) Quantitative comparison in the recovery behavior of quenched $\Delta A_{0\text{-}0}$ during spontaneous de-doping. Sparse hatched-pattern: $\tau_{1/e}$, dense hatched-pattern: $\tau_{90\%}$. c–e) Half-potential cyclic voltammetry as a function of relative potential with Ag/AgCl reference electrode. Sweep rate: 20 mV s^{-1}.

change $\Delta A_{0\text{-}0}$ in absorbance at the 0-0 transition peak and the change ΔA_{1000nm} in absorbance at $\lambda = 1000$ nm (**Figure 3**a). Here, ΔA_{1000nm} was considered as an indirect indicator of the formation and disappearance of the polaronic state, because the absorption of polaronic states in DPP copolymer films occurs in the broad range of near-infrared region.

During electrochemical doping ($t < 40$ s), $A_{0\text{-}0}$ decreased rapidly and A_{1000nm} increased rapidly in the DPP-blend film; these trends are consistent with the trends in EPSC at $V_G = -2.5$ V (Figure 2d–f). The facile doping of anions into DPP-blend film creates the largest quantity of hole compensation, resulting in the strongest quenching in 0-0 transition peak and an increase in the quantity of polaronic species. Moreover, in the de-doping regime, the DPP-blend film showed the slowest recovery in both absorbances compared to the other films. This indicates that the blend film has the slowest back-diffusion of doped anions and the corresponding slowest disappearance of generated polaronic states in the polymer backbone than either single-component film.

For a quantitative comparison of the back-diffusion kinetics of anions, two time-constants were calculated from the recovery of $A_{0\text{-}0}$ in the de-doping regime (Figure 3b). Time constant $\tau_{1/e}$ is the time needed for the changed absorbance to decay to $1/e$ of the difference between maximum and steady-state values, and $\tau_{90\%}$

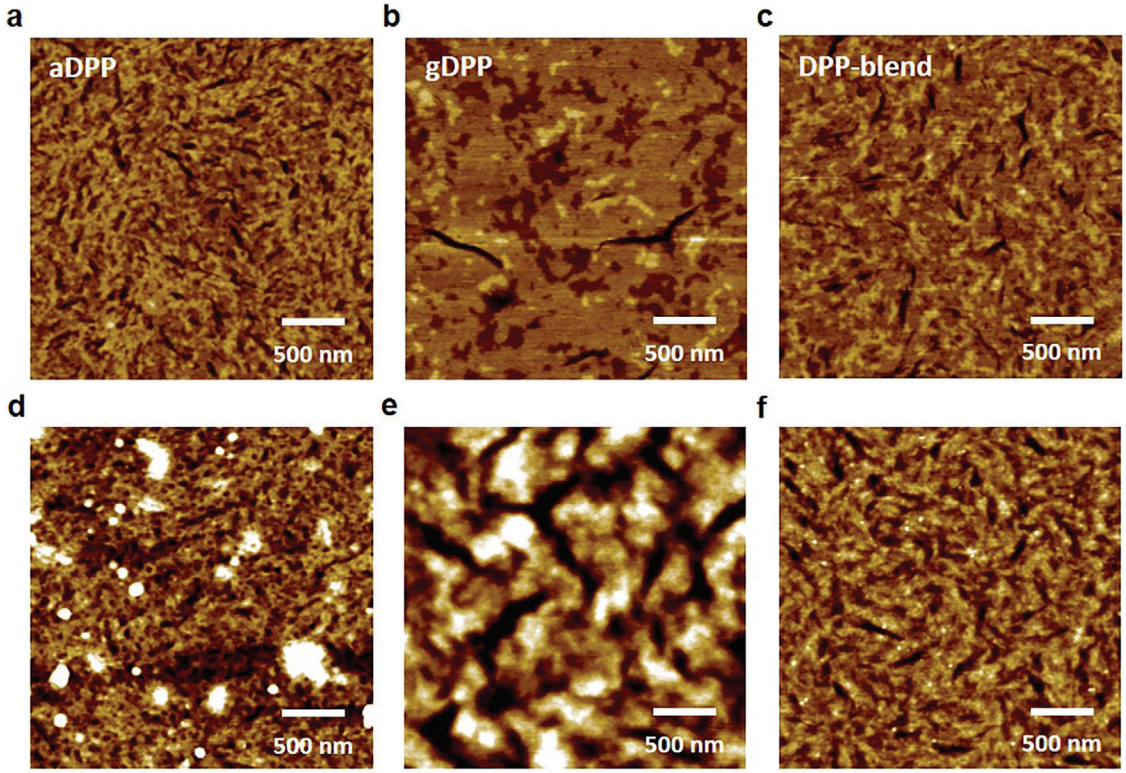

Figure 4. Atomic force microscopy (AFM) images of DPP copolymer films. Topographies for pristine dry films of a) aDPP, b) gDPP, and c) DPP-blend copolymers. Topographies for electrochemically doped films of d) aDPP, e) gDPP, and f) DPP-blend copolymers. *Ex situ* electrochemical doping was performed in an aqueous electrolyte (0.1 M LiTFSI).

is the time required to complete 90% of this decay. The tendencies of $\tau_{1/e}$ and $\tau_{90\%}$ for DPP copolymer films exactly matched that of the LTP characteristic of the IGPSTs. These results of in situ electrochemical UV-vis spectroscopy are concrete evidence for increased retention time of LTP characteristics in $IGPST_{A+G}$.

Cyclic voltammetry was conducted to compare the polymer-ion interactions of each polymer film as it oxidizes. The cyclic voltammogram (CVgram) of the thin film of aDPP copolymer did not show any clear oxidation peak within the potential range from 0 to 2.5 V (Figure 3c). The CVgram of gDPP film showed a clear first oxidation peak at 0.9 V and a relatively weak second oxidation peak at 1.9 V (Figure 3d). The obvious oxidation peaks appear because ethylene glycol end groups boost the efficiency of bulk-ion injection and facilitate electrochemical reactions with the doped anions.[29,30] Concurrently, gDPP copolymer chains in gDPP film swelled by absorbing the liquid electrolyte; this phenomenon caused the passive uptake of mobile ions, and as a consequence, the film had a high capacitive current.[31–34] The CVgram of DPP-blend film showed distinct oxidation peaks at 0.8 and 1.7 V (Figure 3e). The oxidation potentials were further lower in DPP-blend film than in gDPP film; this change confirmed that electrochemical doping is easier in the blended system of alkyl and glycolated side chains than in the presence of only glycolated side chains.

The amplitude of the oxidation peak currents was higher in the DPP-blend film than in the gDPP film. This result demonstrates that aDPP and gDPP copolymer chains can create stronger redox reactions with doped ions in DPP-blend film than either in aDPP or gDPP films.[31] This finding was surprising because the number of electroactive sites (i.e., oligo ethylene glycol (OEG) group) is greater in the gDPP film than in the blend film. Moreover, relative to the gDPP film, the introduction of hydrophobic alkyl side chains by the blending method greatly decreased the capacitive current. These results indicate that the presence of both aDPP and gDPP copolymer chains strengthened the redox reactions between doped anions and polymer chains while reducing the passive uptake of ions and swelling of gDPP copolymer chains. The strengthened redox reaction and reduced capacitive current can be explained by restricted morphological changes upon electrochemical doping.[32,35] Subsequent *ex situ* electrochemical atomic force microscopy (EC-AFM) further explained this phenomenon.

Ex situ EC-AFM was conducted to elucidate the morphological change upon the electrochemical doping in the films. To conduct *ex situ* EC-AFM, each DPP copolymer film was subjected to an electrochemical reaction of in an aqueous electrolyte of 0.1 M LiTFSI (Figure S16, Supporting Information). Before the electrochemical doping, the surface of all pristine thin films was smooth showing low surface roughness $1.1 \leq R_q \leq 1.3$ nm. The aDPP thin film exhibited nano-fibrillar topography (**Figure** 4a), the gDPP thin film had granular and smoother surface (Figure 4b), and DPP-blend thin film had coexisting fibrillar and granular microstructure (Figure 4c).

Electrochemical doping affected the DPP copolymer films differently. The aDPP film remained almost unaltered from its dry

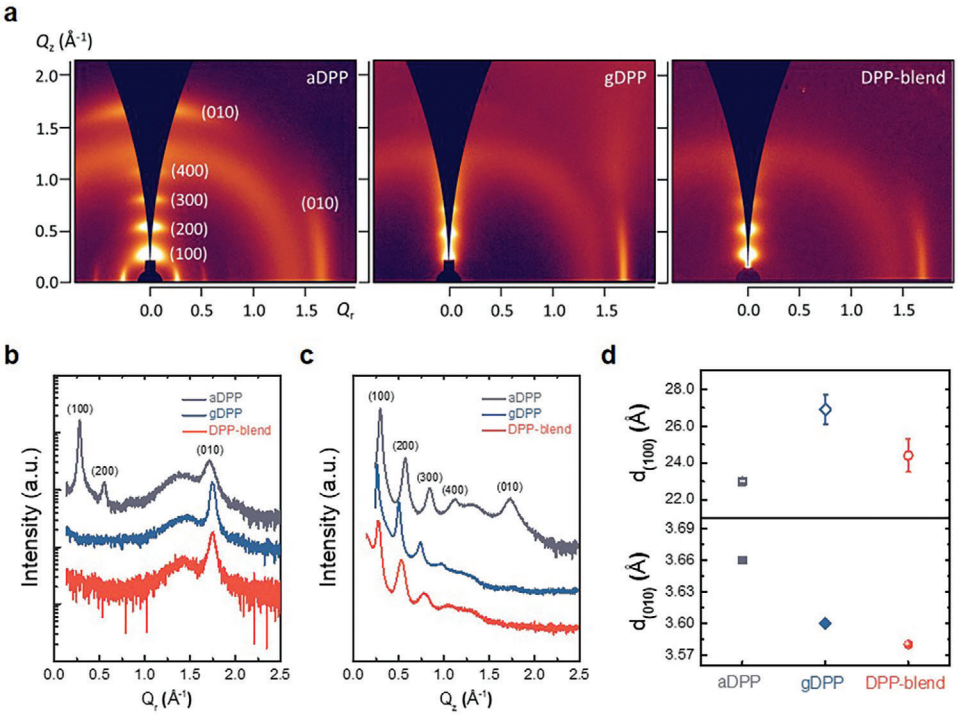

Figure 5. Grazing incidence X-ray diffraction (GIXD) measurement of DPP copolymer thin films. a) 2D GIXD patterns of the DPP copolymer thin films. 1D GIXD diffractograms of the DPP copolymer thin films with respect to b) out-of-plane Q_z axis and c) in-plane Q_r axis. d) Lamellar d-spacing ($d_{(100)}$, open symbols) and π-π stacking distance ($d_{(010)}$, closed symbols) of the DPP copolymer thin films, calculated from 1D GIXD diffractograms. Grey line/square dot: aDPP film, blue line/rhombus dot: gDPP film, red line/sphere dot: DPP-blend film.

state, with a slight increase of R_q from 1.3 to 1.9 nm (Figure 4d); the reason that the change is small may be that the hydrophobicity of alkyl side chains almost prevented the water uptake of aDPP film. In contrast, gDPP film significantly expanded during the doping, and developed an evident heterogeneous pattern on its surface, which is a result of a high degree of swelling by the polar and hydrophilic ethylene glycol side chains during electrochemical operation (Figure 4e).[32,33,36] As a result, R_q of gDPP film increased from 1.1 to 3.0 nm. DPP-blend film swelled with slightly increased R_q from 1.2 to 1.6 nm and well-distributed fibril-like patterns appeared (Figure 4f).

The DPP-blend film did not develop the heterogeneous pattern observed in the gDPP film, and morphological alterations in the blend film were strongly constrained during electrochemical doping. This phenomenon may be a result of steric suppression of glycolated sidechain expansion by the adjacent alkyl side chains.[35] Furthermore, the results from *ex situ* EC-AFM and the observed improvement in the retention behavior of $IGPST_{A+G}$ align with a previous study, which noted that substantial changes in film morphology during electrochemical operation can cause low state-retention.[37] Hence, we consider that the blend strategy contributes to the restriction of morphological changes during electrochemical doping, and therefore reduces capacitive current, strengthens redox reactions, and suppresses the de-doping of anions (Figure 2 and Figure 3c–e).

To identify the packing structure of DPP copolymers in each film, grazing incidence X-ray diffraction (GIXD) was performed. For aDPP thin film, several scattering peaks related to the lamellar spacing of (h00) planes and π-π stacking distance of (010) plane were observed along the out-of-plane Q_z and in-plane Q_r directions. This result indicates that aDPP copolymers are arranged in mixed edge-on and face-on orientations. In contrast, gDPP and DPP-blend films showed only scattering peaks related to π-π stacking distance of the (010) plane along the in-plane direction; this result indicates that they are in the edge-on orientation (**Figure 5**a–c). The evolution toward the edge-on orientation as glycolation of side chains may occur because it reduces steric hindrance and side-chain density.[30,38] 1D diffractograms indicate that the lamellar spacing of the (100) plane in gDPP film was 2.69 nm, which is larger than that in aDPP film (2.30 nm) (Figure 5d). The difference is attributed to the longer side chains in gDPP than in aDPP.[39]

The DPP-blend film showed a single scattering peak of (100) plane and a lamellar spacing between those of aDPP and gDPP films (Figure 5b–d). This result indicates that a blending of the two DPP copolymers yielded well intermixed phase in the solid-state thin film.[47] In addition, blending caused a significant decrease in the domain size D_C of well-ordered regions, because blending yields well-developed intermixing between aDPP and gDPP copolymers (**Table 1**).[40,41]

Comparison of the π-π stacking distances indicates that gDPP thin film had denser backbone stacking than aDPP thin film; the difference occurs because glycolated side chains have both higher flexibility and lower steric hindrance than alky side chains.[42] The DPP-blend thin film had a much lower π-π stacking distance than the aDPP and gDPP thin films (Figure 5d). Therefore, GIXD measurement demonstrates that blending these two PSCs that have the same backbone might establish well-developed

Table 1. The structural information obtained from the GIXD measurement.

DPP films	$\Delta Q_{[100]}$ [a)] [Å^{-1}]	$D_{[100]}$ [Å]	$Q_{[010]}$ [b)] [Å^{-1}]	$D_{[010]}$ [Å]	FWHM at $Q_{[200]}$ [c)] [Å^{-1}]	D_c [d)] [nm]
aDPP film	0.2734	23.0	1.715	3.66	0.0464	26.9
gDPP film	0.2339	26.9	1.746	3.60	0.0361	31.4
DPP-blend film	0.2572	24.4	1.756	3.58	0.0661	17.1

[a)] Extracted from the 1D GIXD linecut along out-of-plane direction; [b)] Extracted from the 1D GIXD linecut along in-plane direction; [c)] Determined from the d-spacing of $(200)_{edge\text{-}on}$ planes; [d)] Grain size (D_c) = $\kappa\cdot\lambda/\beta cos\theta$, $\kappa = 0.9$, $\lambda = 0.10\,722$ nm (the wavelength of the X-ray), β: FWHM width of the diffraction peak, θ: diffraction angle [Scherrer equation].

intermixing that minimizes adverse effects on the conjugated backbone and electronic charge transport. Moreover, although DPP-blend thin film had the lowest crystallinity considering the weak scattering peak intensities of (h00) planes, $IGPST_{A+G}$ showed the longest retention of LTP among the IGPSTs (Figure 2). This result indicates that the change in crystallinity was not responsible for the increased retention time of LTP.[5,15]

Recognition with an artificial neural network (ANN) was simulated with $IGPST_A$, $IGPST_G$, and $IGPST_{A+G}$ to evaluate the applicability of the blending method. The ANN consisted of 784 input neurons, 100 hidden neurons, and 10 output neurons to classify handwritten digit images of size 28 × 28 pixels (**Figure 6a**). The conductance G_i states of the IGPSTs, which represent the synaptic weight in ANN, were adjusted by applying 50 consecutive potentiation spikes, for the write and then 50 depression spikes for the erase operation. The nonlinearity $|\nu|$ is an important feature that quantifies the uniformity of conductance change.[2,43] $|\nu|$ can be fitted for potentiation curves as

$$G_{P,i} = G_1\left(1 - e^{-\nu P}\right) + G_{min}, \quad G_1 = \frac{G_{max} - G_{min}}{1 - e^{-\nu}} \tag{4}$$

and for depression curves as

$$G_{D,i} = G_2\left(1 - e^{-\nu P}\right) + G_{max}, \quad G_2 = -\frac{G_{max} - G_{min}}{1 - e^{-\nu}} \tag{5}$$

where P is a state number normalized by the total number of states, $G_{P,i}$ represents conductance states after the i^{th} potentiation, and $G_{D,i}$ represents the state after depression (i = 1, 2, 3, ..., 50), G_{max} is the maximum of G_i in the range of 50 conductance states, and G_{min} is its minimum value.[44]

IGPSTs are afflicted by read noise because their operating mechanism involves spontaneous de-doping of doped ions and continuous decay of EPSC. To minimize this noise, a sufficient read time was chosen to ensure that each conductance state reached the saturation regime (Figure S17, Supporting Information). In all three IGPSTs, potentiation curves were more linear than depression curves; this difference is a common phenomenon in synaptic devices that use electrolyte gating because it is accompanied by spontaneous back-diffusion of doped anions during device operation.[45,46] $IGPST_{A+G}$, which had the highest retention time showed $|\nu| = 0.6$ for potentiation curves, and 5.9 for depression curves, whereas $IGPST_A$, which had the lowest retention time, showed $|\nu| = 1.9$ for potentiation curves and 7.8 for depression curves (Figure 6b–d). The observed trend in the linearity of the depression curve might be linked to the improved ability of DPP-blend film to capture doped ions during the early stages of depression. All IGPSTs exhibited a large dynamic range (up to 10^3) and low cycle-to-cycle variation over more than 10^3 operations (Figure S18, Supporting Information). Each conductance state was consistently maintained throughout cyclic operations, affirming the low process noise and the reliability of multiple conductance states in each IGPST (Figure S19, Supporting Information).

The ANN was trained using the MNIST dataset in crossbar simulations. All three IGPSTs achieved training accuracies obtained from the recognition simulation > 90% of large digits (28 × 28 pixels) after 40 epochs training. The high training accuracies may occur because all three IGPSTs have high dynamic range and low cycle-to-cycle variation.[47] $IGPST_{A+G}$ achieved a training accuracy of 96.8%, which is comparable to the ideal numerical value (98.2%) (Figure 6e), whereas $IGPST_A$ achieved a training accuracy of 92.7% and $IGPST_G$ achieved 93.3%. The highest training accuracy of $IGPST_{A+G}$ is a result of its lowest nonlinearity in the multi-conductance curves. Consequently, the highest retention time of LTP in $IGPST_{A+G}$ resulted in the highest training accuracy in the ANN simulation. These results prove that extending the LTP by the blending method is a valid strategy for implement IGPSTs for neuromorphic applications.

3. Conclusion

This study has provided a general strategy for achieving long retention time T_{rtn} of LTP without any adverse effect on electrochemical doping efficiency η_{echem} by obtaining a well-intermixed PSC blend of two different PSCs that have the same backbone but different types of side chains (alkyl and glycolated side chains). The high η_{echem} could be preserved because the environments for electronic charge transport such as dense π-π backbone stacking were maintained. The increased T_{rtn} of LTP characteristic in the blend film was supported by the slowest recovery of quenched 0-0 transition peak after electrochemical doping in the in situ electrochemical UV-vis spectroscopy. Blending of hydrophobic and rigid alkyl side chain with hydrophilic and flexible ethylene glycolated side chain can suppress the relaxation of ethylene glycol side chains. Therefore, in the blend film, this change strengthens the redox activity of copolymers with doped ions during electrochemical doping, which could potentially explain the retarded back-diffusion of doped ions (and the prolonged retention of LTP). Finally, multi-conductance states were measured to evaluate the efficiency of the blending method in recognition simulation with ANNs. The linearity of potentiation and depression

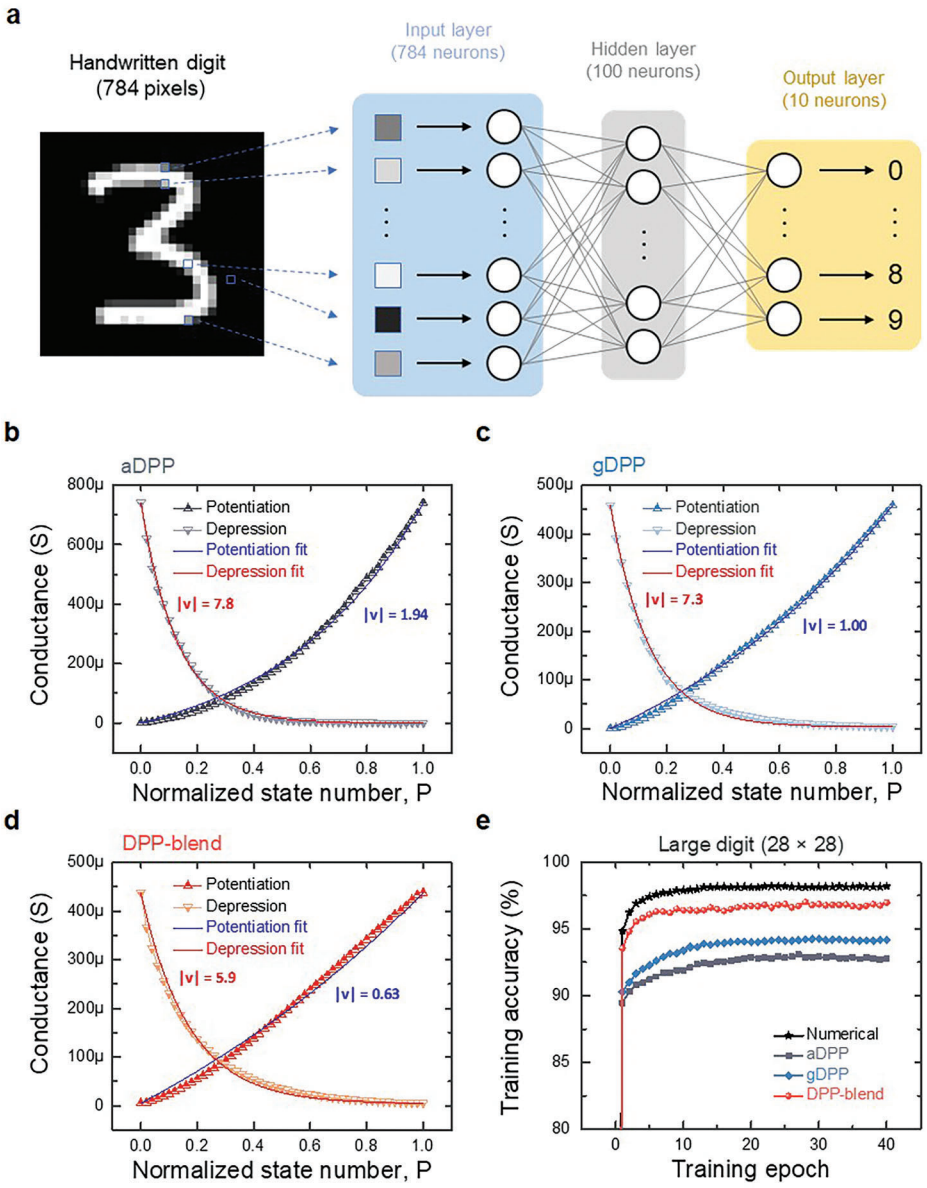

Figure 6. Multi-conductance states and simulation for MNIST handwritten digit recognition. a) Schematic of the artificial neural network (ANN) used to run the simulation. Multi-conductance states of b) $IGPST_A$, c) $IGPST_G$, and d) $IGPST_{A+G}$ with 50 potentiation spikes (up-pointing triangle) and depression (down-pointing triangle) presynaptic spikes. Potentiation spikes: −3.5 V, 200 ms for $IGPST_A$, −3.5 V, 100 ms for $IGPST_G$, and −3.0 V, 100 ms for $IGPST_{A+G}$. Depression spikes: 3.0 V, 100 ms for $IGPST_A$, 2.5 V, 100 ms for $IGPST_G$, and 2.5 V, 100 ms for $IGPST_{A+G}$. In all cases, $V_D = -100$ mV was applied to read the conductance state within consecutive presynaptic spikes. All conductance states were fitted to define the linearity parameter $|\nu|$ of potentiation curve (blue solid line) and depression curve (red solid line). e) Training accuracy of ideal numerical device (black dot), $IGPST_A$ (grey square dot), $IGPST_G$ (blue rhombus dot), and $IGPST_{A+G}$ (red round dot) with respect to training epochs for 28 × 28-pixel images of digits.

curves was improved by exploiting IGPST with the blend film so that high training accuracy (96.8%) comparable to the ideal numerical value (98.2%) was achieved.

To the best knowledge of the authors, this is the first successful achievement of prolonged retention time of LTP with maintaining high efficiency of electrochemical doping despite the crystallinity decreased by blending two PSCs. This method provides a promising method to modulate synaptic plasticity and is applicable to diverse neuromorphic devices.[48–50]

4. Experimental Section

Materials and Synthesis: All chemicals and solvent for the synthesis of DPP copolymers were purchased form TCI, Alfa aesar and Aldrich. All reagent purchased commercially were used without further purification. PDPP-TTVTT-β-$C_{10}C_{12}$ (poly[2,5-bis(2-decyltetradecyl)pyrrolo[3,4-c]pyrrole-1,4-(2H,5H)-dione-(E)−1,2-di(2,2′-bithiophen-5-yl)ethene])[51] (M_n = 78.3 kDa, M_w = 155.5 kDa PDI = 1.98), PDPP-TTVTT-C_{12}-TEG (poly[2,5-bis(2,5,8,11-tetraoxatricosan-23-yl)pyrrolo[3,4-c]pyrrole-1,4-(2H,5H)-dione-(E)−1,2-di(2,2′-bithiophen-5-yl)ethene])[19] (M_n = 64 kDa, M_w = 71.2 kDa, PDI = 1.11) were synthesized by reported

methods. The polymer was purified by successive Soxhlet extractions with acetone, methanol, and hexane to remove the metal catalyst. Then the polymer dissolved in chloroform was precipitated into methanol. The molecular weight of polymers was measured by GPC using polystyrene standard in chloroform solvent. The other experimental materials including poly(vinylidene fluoride-co-hexafluoropropylene) (PVDF-HFP) (Mw = 400000), 1-ethyl-3-methylimidazolium bis(trifluoromethylsulfonyl) imide ([EMIM][TFSI]), bis(trifluoromethane)sulfonimide lithium salt (LiTFSI), acetone, and chloroform were purchased from Sigma Aldrich.

Device Fabrication: DPP copolymer thin films were spin-coated from a solution of chloroform (5 mg mL^{-1}) on a Si/SiO_2 (100 nm) substrate at 1000 rpm for 60 s, then thermally annealed at 220 °C for 30 min under N_2 atmosphere. Au was thermally deposited to form source and drain electrodes (30 nm) by using a patterned shadow mask under vacuum ($\approx 10^{-6}$ Torr). The defined channel was 50 μm long and 1.5 mm wide (W/L = 30). The thickness was 40 nm for aDPP film, 35 nm for gDPP film, and 45 nm for DPP-blend film. Ion gel composed of PVDF-HFP and [EMIM][TFSI] in acetone (1:4:11, w:w:w) was drop cast on bare glass substrate then dried at 80 °C for 1 h. The dried ion-gel was cut to fit the channel size and transferred to the top of the channel (called "cut-and-paste" method). The thickness of the dried ion-gel was 5 µm, so conformal contact with the channel polymer was assured. The thicknesses of all polymer films and dried ion gels were measured using a DektakXT-E Stylus profiler.

Characterization of Synaptic Properties: All synaptic properties of ion-gel gated polymer synaptic transistors (IGPSTs) were measured using a Keithley 2600. An Au tip was used to establish a gate contact with the ion-gel electrolyte. *I–V* sweeps of V_G = 3.5 to–3.5 V (forward) and −3.5 V to 3.5 V (backward) were conducted at sweep rates of 100 mV s^{-1} under N_2 atmosphere. During characterization of synaptic properties, V_D was −100 mV, and the duration was 100 ms. Hysteresis in transfer curves was estimated as the voltage difference between two gate voltages at current equal to half of the maximum I_{on} during forward and backward sweeps.

In Situ UV-vis Spectroscopy: DPP copolymer thin films were prepared (using the same methods as in previous sections) on glass coated with indium tin oxide (ITO). Then the solidified ion-gel was cut-and-pasted on top of DPP copolymer thin films. In situ UV-vis absorption spectra were obtained using a PerkinElmer Lambda 465 UV-vis Spectrophotometer. A Keithley 2600 source meter was used to apply bias to the solidified ion gel and ground voltage to the ITO bottom electrode.

Cyclic Voltammetry: A 30-nm-thick layer of Au was thermally deposited on bare glass substrate in high vacuum ($\approx 10^{-6}$ Torr). Then DPP copolymers were deposited on Au film (using the same deposition parameters as in the previous section). Pt counter electrode, Ag/AgCl reference electrode, and Au working electrode coated with DPP copolymer were immersed in acetone electrolyte (0.1 M [EMIM][TFSI]). Cyclic voltammetry measurements were conducted using an EC-Lab potentiostat SP-300 to apply an oxidizing-potential range between 0 and 2.5 V with respect to the Ag/AgCl reference, at a sweep rate of 20 mV s^{-1}.

Ex Situ Electrochemical Atomic Force Microscopy (EC-AFM): DPP copolymer thin films were prepared as in previous sections on a native Si substrate. For ex situ electrochemical doping, Pt electrode and DPP copolymer thin film were immersed in aqueous electrolyte (0.1 M LiTFSI). Continuous bias of −1.5 V was applied to the Pt electrode by a Keithley 2600 source meter, then the DPP copolymer thin film was immediately removed from the electrolyte and dried by blowing N_2 gas over it. AFM and ex situ electrochemical AFM were conducted using a Multimode 8 (Park System). All AFM measurements were performed in tapping mode.

Grazing-Incidence X-ray Diffraction (GIXD): GIXD was performed on the films at beamlines 6D and 9A of the Pohang Accelerator Laboratory (PAL), Republic of Korea. The incident angle of the X-ray beam (λ = 1.0722 Å) on a sample was fixed at 0.12°.

Crossbar Array Simulation: A crossbar array was simulated using Cross-sim (Sandia National Laboratory, USA). A three-layer (784 × 100 × 10) network was used to analyze datasets of MNIST images. Training used 60000 handwritten digits, and recognition testing used 10000 handwritten digits. The learning rate was 0.05 for numerical calculations and the IGPSTs.

Supporting Information

Supporting Information is available from the Wiley Online Library or from the author.

Acknowledgements

This work was supported by the Creative-Pioneering Researchers Program through the National Research Foundation of Korea (NRF) grant funded by the Korea government (Ministry of Science and ICT) (grant no. NRF-2016R1A3B1908431), the Pioneer Research Center Program through the National Research Foundation of Korea (NRF) funded by the Ministry of Science, ICT & Future Planning (grant no. NRF-2022M3C1A3081211), and the National R&D Program through the National Research Foundation of Korea (NRF) funded by Ministry of Science and ICT (2021M3F3A2A01037858).

Conflict of Interest

The authors declare no conflict of interest.

Author Contributions

M.-J. S., D.-G. S., and T.-W. L. conceived the research idea and co-wrote the paper. J. K., H. E. B., and Y.-H. K. synthesized the experimental materials. M.-J. S. designed and conducted the overall experiments with the help of D.-G. S., S.-J. W., G.-T. G., and K.-N. K.. H. Y. performed GIXD measurements. T.-W. L. initiated and supervised the project. All authors discussed the results and commented on the manuscript.

Data Availability Statement

The data that support the findings of this study are available from the corresponding author upon reasonable request.

Keywords

blending polymer semiconductors, efficient electrochemical doping, high state retention, restriction of morphological changes, side chain engineering

Received: October 11, 2023
Revised: November 19, 2023
Published online:

[1] Y. Van De Burgt, P. Gkoupidenis, *MRS Bull.* **2020**, *45*, 631.
[2] Y. Van De Burgt, A. Melianas, S. T. Keene, G. Malliaras, A. Salleo, *Nat. Electron.* **2018**, *1*, 386.
[3] Y. Lee, T.-W. Lee, *Acc. Chem. Res.* **2019**, *52*, 964.
[4] Y. Zheng, S. Zhang, J. B.-H. Tok, Z. Bao, *J. Am. Chem. Soc.* **2022**, *144*, 4699.
[5] G.-T. Go, Y. Lee, D.-G. Seo, M. Pei, W. Lee, H. Yang, T.-W. Lee, *Advanced Intelligent Systems* **2020**, *2*, 2000012.
[6] P. Gkoupidenis, N. Schaefer, X. Strakosas, J. A. Fairfield, G. G. Malliaras, *Appl. Phys. Lett.* **2015**, *107*, 263302.
[7] H. Han, H. Yu, H. Wei, J. Gong, W. Xu, *Small* **2019**, *15*, 1900695.
[8] H. Ling, D. A. Koutsouras, S. Kazemzadeh, Y. Van De Burgt, F. Yan, P. Gkoupidenis, *Appl. Phys. Rev.* **2020**, *7*, 011307.

[9] F. Torricelli, D. Z. Adrahtas, Z. Bao, M. Berggren, F. Biscarini, A. Bonfiglio, C. A. Bortolotti, C. D. Frisbie, E. Macchia, G. G. Malliaras, I. Mcculloch, M. Moser, T.-Q. Nguyen, R. M. Owens, A. Salleo, A. Spanu, L. Torsi, *Nature Reviews Methods Primers* **2021**, *1*, 66.
[10] J. Lee, L. G. Kaake, J. H. Cho, X.-Y. Zhu, T. P. Lodge, C. D. Frisbie, *J. Phys. Chem. C* **2009**, *113*, 8972.
[11] J. H. Cho, J. Lee, Y. Xia, B. Kim, Y. He, M. J. Renn, T. P. Lodge, C. Daniel Frisbie, *Nat. Mater.* **2008**, *7*, 900.
[12] J. H. Cho, J. Lee, Y. He, B. S. Kim, T. P. Lodge, C. D. Frisbie, *Adv. Mater.* **2008**, *20*, 686.
[13] H.-L. Park, Y. Lee, N. Kim, D.-G. Seo, G.-T. Go, T.-W. Lee, *Adv. Mater.* **2020**, *32*, 1903558.
[14] H. Han, Z. Xu, K. Guo, Y. Ni, M. Ma, H. Yu, H. Wei, J. Gong, S. Zhang, W. Xu, *Adv. Intell. Syst.* **2020**, *2*, 1900176.
[15] D.-G. Seo, Y. Lee, G.-T. Go, M. Pei, S. Jung, Y. H. Jeong, W. Lee, H.-L. Park, S.-W. Kim, H. Yang, C. Yang, T.-W. Lee, *Nano Energy* **2019**, *65*, 104035.
[16] X. Ji, B. D. Paulsen, G. K. K. Chik, R. Wu, Y. Yin, P. K. L. Chan, J. Rivnay, *Nat. Commun.* **2021**, *1*, 2480.
[17] H. Frankenstein, E. Stein, M. Stolov, M. Koifman Khristosov, V. Freger, G. L. Frey, *J. Mater. Chem. C* **2021**, *9*, 7765.
[18] I. Kang, H.-J. Yun, D. S. Chung, S.-K. Kwon, Y.-H. Kim, *J. Am. Chem. Soc.* **2013**, *135*, 14896.
[19] E. Tan, J. Kim, K. Stewart, C. Pitsalidis, S. Kwon, N. Siemons, J. Kim, Y. Jiang, J. M. Frost, D. Pearce, J. E. Tyrrell, J. Nelson, R. M. Owens, Y.-H. Kim, J.-S. Kim, *Adv. Mater.* **2022**, *34*, 2202574.
[20] J. Nightingale, C. Pitsalidis, A.-M. Pappa, E. Tan, K. Stewart, R. M. Owens, J.-S. Kim, *J. Mater. Chem. C* **2020**, *8*, 8846.
[21] K. G. Cho, K. H. Seol, M. S. Kim, K. Hong, K. H. Lee, *ACS Appl. Mater. Interfaces* **2022**, *14*, 50004.
[22] J. T. Friedlein, R. R. Mcleod, J. Rivnay, *Org. Electron.* **2018**, *63*, 398.
[23] M. Xie, H. Liu, M. Wu, C. Chen, J. Wen, L. Bai, J. Yu, W. Huang, *Org. Electron.* **2023**, *117*, 106777.
[24] R. S. Zucker, W. G. Regehr, *Annu. Rev. Physiol.* **2002**, *64*, 355.
[25] L. Bao, J. Zhu, Z. Yu, R. Jia, Q. Cai, Z. Wang, L. Xu, Y. Wu, Y. Yang, Y. Cai, R. Huang, *ACS Appl. Mater. Interfaces* **2019**, *11*, 41482.
[26] J. Lee, L. G. Kaake, J. H. Cho, X. Zhu, T. P. Lodge, C. D. Frisbie, *J. Phys. Chem. C* **2009**, *113*, 8972.
[27] S. Wood, J. Wade, M. Shahid, E. Collado-Fregoso, D. D. C. Bradley, J. R. Durrant, M. Heeney, J.-S. Kim, *Energy Environ. Sci.* **2015**, *8*, 3222.
[28] Y. Wang, A. Hamidi-Sakr, J. Surgailis, Y. Zhou, H. Liao, J. Chen, G. Zhu, Z. Li, S. Inal, W. Yue, *J. Mater. Chem. C* **2021**, *9*, 13338.
[29] A. Giovannitti, D. Sbircea, S. Inal, C. B. Nielsen, E. Bandiello, *PNAS* **2016**, *113*, 12017.
[30] C. B. Nielsen, A. Giovannitti, D. Sbircea, E. Bandiello, M. R. Niazi, D. A. Hani, M. Sessolo, A. Amassian, G. G. Malliaras, J. Rivnay, I. Mcculloch, *J. Am. Chem. Soc.* **2016**, *138*, 10252.
[31] M. Moser, L. R. Savagian, A. Savva, M. Matta, J. F. Ponder, T. C. Hidalgo, D. Ohayon, R. Hallani, M. Reisjalali, A. Troisi, A. Wadsworth, J. R. Reynolds, S. Inal, I. Mcculloch, *Chem. Mater.* **2020**, *32*, 6618.
[32] A. Savva, R. Hallani, C. Cendra, J. Surgailis, T. C. Hidalgo, S. Wustoni, R. Sheelamanthula, X. Chen, M. Kirkus, A. Giovannitti, A. Salleo, I. Mcculloch, S. Inal, *Adv. Funct. Mater.* **2020**, *30*, 1907657.
[33] A. Giovannitti, I. P. Maria, D. Hanifi, M. J. Donahue, D. Bryant, K. J. Barth, B. E. Makdah, A. Savva, D. Moia, M. S. Zetek, P. R. F. Barnes, O. G. Reid, S. Inal, G. Rumbles, G. G. Malliaras, J. Nelson, J. Rivnay, I. Mcculloch, *Chem. Mater.* **2018**, *30*, 2945.
[34] J. Chen, W. Huang, D. Zheng, Z. Xie, X. Zhuang, D. Zhao, Y. Chen, N. Su, H. Chen, R. M. Pankow, Z. Gao, J. Yu, X. Guo, Y. Cheng, J. Strzalka, X. Yu, T. J. Marks, A. Facchetti, *Nat. Mater.* **2022**, *21*, 564.
[35] A. A. Szumska, I. P. Maria, L. Q. Flagg, A. Savva, J. Surgailis, B. D. Paulsen, D. Moia, X. Chen, S. Griggs, J. T. Mefford, R. B. Rashid, A. Marks, S. Inal, D. S. Ginger, A. Giovannitti, J. Nelson, *J. Am. Chem. Soc.* **2021**, *143*, 14795.
[36] A. Savva, C. Cendra, A. Giugni, B. Torre, J. Surgailis, D. Ohayon, A. Giovannitti, I. McCulloch, E. Di Fabrizio, A. Salleo, J. Rivnay, S. Inal, *Chem. Mater.* **2019**, *31*, 927.
[37] S. J. Kim, J.-S. Jeong, H. W. Jang, H. Yi, H. Yang, H. Ju, J. A. Lim, *Adv. Mater.* **2021**, *33*, 2100475.
[38] Z. Wang, Z. Liu, L. Ning, M. Xiao, Y. Yi, Z. Cai, A. Sadhanala, G. Zhang, W. Chen, H. Sirringhaus, D. Zhang, *Chem. Mater.* **2018**, *30*, 3090.
[39] J. Liu, G. Ye, H. G. O. Potgieser, M. Koopmans, S. Sami, M. I. Nugraha, D. R. Villalva, H. Sun, J. Dong, X. Yang, X. Qiu, C. Yao, G. Portale, S. Fabiano, T. D. Anthopoulos, D. Baran, R. W. A. Havenith, R. C. Chiechi, L. J. A. Koster, *Adv. Mater.* **2021**, *33*, 2006694.
[40] H. Kang, M. A. Uddin, C. Lee, K.-H. Kim, T. L. Nguyen, W. Lee, Y. Li, C. Wang, H. Y. Woo, B. J. Kim, *J. Am. Chem. Soc.* **2015**, *137*, 2359.
[41] Y. Wu, S. Schneider, C. Walter, A. H. Chowdhury, B. Bahrami, H.-C. Wu, Q. Qiao, M. F. Toney, Z. Bao, *J. Am. Chem. Soc.* **2020**, *142*, 392.
[42] B. Meng, H. Song, X. Chen, Z. Xie, J. Liu, L. Wang, *Macromolecules* **2015**, *48*, 4357.
[43] G. W. Burr, R. M. Shelby, S. Sidler, C. Di Nolfo, J. Jang, I. Boybat, R. S. Shenoy, P. Narayanan, K. Virwani, E. U. Giacometti, B. N. Kurdi, H. Hwang, *IEEE Trans. Electron Devices* **2015**, *62*, 3498.
[44] S. T. Keene, A. Melianas, E. J. Fuller, Y. Van De Burgt, A. A. Talin, A. Salleo, *J. Phys. D: Appl. Phys.* **2018**, *51*, 224002.
[45] S. Oh, J. H. Lee, S. Seo, H. Choo, D. Lee, J. I. Cho, J. H. Park, *Adv. Sci.* **2022**, *9*, 2103808.
[46] G. Liu, Q. Li, W. Shi, Y. Liu, K. Liu, X. Yang, M. Shao, A. Guo, X. Huang, F. Zhang, Z. Zhao, Y. Guo, Y. Liu, *Adv. Funct. Mater.* **2022**, *32*, 2200959.
[47] Y. Li, T. P. Xiao, C. H. Bennett, E. Isele, A. Melianas, H. Tao, M. J. Marinella, A. Salleo, E. J. Fuller, A. A. Talin, *Front. Neurosci.* **2021**, *15*, 636127.
[48] Y. Kim, A. Chortos, W. Xu, Y. Liu, J. Y. Oh, D. Son, J. Kang, A. M. Foudeh, C. Zhu, Y. Lee, S. Niu, J. Liu, R. Pfattner, Z. Bao, T.-W. Lee, *Science* **2018**, *360*, 998.
[49] Y. Lee, J. Y. Oh, W. Xu, O. Kim, T. R. Kim, J. Kang, Y. Kim, D. Son, J. B. H. Tok, M. J. Park, Z. Bao, T. W. Lee, *Sci. Adv.* **2018**, *4*, eaat7387.
[50] I. Krauhausen, D. A. Koutsouras, A. Melianas, S. T. Keene, K. Lieberth, H. Ledanseur, R. Sheelamanthula, A. Giovannitti, F. Torricelli, I. McCulloch, P. W. M. Blom, A. Salleo, Y. van de Burgt, P. Gkoupidenis, *Sci. Adv.* **2021**, *7*, eabl5068.
[51] J. H. Lee, Y. H. Lee, Y. H. Ha, J. Kwon, S. Pyo, Y.-H. Kim, W. H. Lee, *RSC Adv.* **2017**, *7*, 7526.